AMSE JOURNALS –2016-Series: Modelling B; Vol. 85; N° 1; pp 28-42
Submitted Oct. 2015; Revised Jan. 17, 2016; Accepted April 15, 2016

MHD Free Convection and Mass Transfer Flow through a Vertical Oscillatory Porous Plate in a Rotating Porous Medium with Hall, Ion-Slip Currents and Heat Source

Md. Delowar Hossain, Md. Abdus Samad and Md. Mahmud Alam*

Department of Applied Mathematics, University of Dhaka, Dhaka-1000, Bangladesh
*Mathematics Discipline, Khulna University, Khulna-9208, Bangladesh
*Corresponding author: (alam_mahmud2000@yahoo.com)

Abstract

In this paper is an investigation of unsteady oscillatory MHD free convection, heat and mass transfer flow of an electrically conducting viscous incompressible fluid through a porous medium along an infinite vertical porous plate with the effects of Hall and ion-slip currents, heat source in a rotating system under the influence of Soret effect. The plate is assumed to oscillate in time with constant frequency so that the solutions of the boundary layer equations are the same oscillatory type. The governing system of partial differential equations are transformed by usual transformation. The dimensionless equations are then solved numerically by finite difference method. With the help of graphs, the effects of the various important parameters entering into the problem on the primary and secondary velocities, temperature and concentration distributions within the boundary layer are discussed. Also the effects of the appropriate parameters on the skin friction coefficient, rates of heat and mass transfer in terms of the Nusselt and Sherwood numbers are presented graphically.

Key words: MHD, Hall effects, oscillation, rotation, heat source

1. Introduction

The MHD mass transfer flow under the action of strong magnetic field plays a role in astrophysical and geophysical problems. Hall and ion-slip currents are likely to be important in flows of laboratory plasma. In the study of magneto hydrodynamic fluid flow in a rotating system has been motivated by several important problems, such as maintenance and secular variations of earth's magnetic field, the internal rotation rate of sun, the structure of rotating stars, the planetary and solar dynamo problem, centrifugal machines etc. Convection in porous medium has applications in geothermal energy recovery, oil extraction, thermal energy storage and flow through filtering devices. The effects of magnetic field on free convection flow are important in liquid-metals, electrolytes and ionized gases. The thermal physics of hydro magnetic problems with mass transfer is of interest in power engineering and metallurgy. The applications of the effect of Hall current on the fluid flow with variable concentration have been seen in MHD power generators,

astrophysical and meteorological studies as well as in plasma physics. The Hall Effect is due merely to the sideways magnetic force on the drifting free charges. In recent years, the analysis of hydromagnetic flow involving heat and mass transfer in porous medium has attracted the attention of many scholars because of its possible applications in diverse fields of science and technology such as–soilsciences, astrophysics, geophysics, nuclear power reactors etc. In geophysics, it finds its applications in the design of MHD generators and accelerators, underground water energy storage system etc. Effects of Hall current and heat transfer on flow due to a pull of eccentric rotating disk were investigated by Asghar *et al.* (2005). Singh (1983) studied the effects of Hall currents on an oscillatory MHD flow in the Stokes problem past an infinite vertical porous plate. The first exact solution of Navier-Stokes equation with flow of viscous incompressible fluid past a horizontal plate oscillating in its own plane investigated by Stokes (1851). Natural convection effects on Stokes problem was first study by Sondalgekar (1979). The same problem was considered by Revankar (2000) for impulsively started or oscillating plate. Turbatu *et al.* (1998) investigated the flow of an incompressible viscous fluid past an infinite plate oscillating with increasing or decreasing velocity amplitude of oscillation. Gupta *et al.* (2003) have analyzed flow in the Ekman layer on an oscillating plate. Soundalgekar *et al.* (1997) found an exact solution for magnetic free convection flow past an oscillating plate. Mass transfer effects on flow past an oscillating plate considered by Lahurikar *et al.* (1995). The study of heat generation or absorption effects in moving fluids is important in view of several physical problems, such as fluids undergoing exothermic or endothermic chemical reactions. Vajravelu and Hadjinicolaou (1993) studied the heat transfer characteristics in the laminar boundary layer of a viscous fluid over a stretching sheet with viscous dissipation or frictional heating and internal heat generation. Ziaul Haque et al.(2012) studied micropolar fluid behaviors on steady MHD free convection and mass transfer flow with constant heat and mass fluxes, joule heating and viscous dissipation. Das *et al* (2004) have been analyzed finite difference analysis of hydromagnetic flow and heat transfer of an elastico-viscous fluid between tow horizontal parallel porous plate. Haque and Alam(2011) studied micropolar fluid behaviours on unsteady MHD heat and Mass transfer flow with constant heat and mass fluxes, joule heating and viscous dissipation**.** Haque and Alam(2009) have been investigated transient heat and mass transfer by mixed convection flow from a vertical porous plate with induced magnetic field, constant heat and mass fluxes.

In this paper the effects of Hall and ion-slip currents on MHD flow in heat and mass transfer of an electrically conducting incompressible fluid along an infinite oscillatory vertical porous plate with heat source in a rotating system have been considered. Also, the effects of different flow parameters encountered in the equations are studied. The problem is governed by system of coupled non-linear partial differential equations whose exact solution is difficult to obtain. Hence, the problem is solved by finite difference method and is represented graphically.

2. Mathematical model of the flow

Consider the unsteady flow of an electrically conducting incompressible viscous fluid past an infinite vertical porous plate $y = 0$. When the plate velocity $U(t)$ oscillates in time t with a frequency n and is given as $U(t) = U_0(1 + cosnt)$. The flow is assumed to be in the $x-$direction and which is taken along the plate in the upward direction and $y-$axis is normal to it. Initially the

fluids as well as the plate are at rest but for time $t > 0$ the whole system is allowed to rotate with a constant angular velocity Ω about the $y-$axis. Initially, it is considered that the plate as well as the fluid is at the same temperature. Also it is assumed that the temperature of the plate and spices concentration are raised to $T_w (> T_\infty)$ and $C_w (> C_\infty)$ respectively, which are there after maintained constant, where T_w, C_w are temperature and spices concentration at the wall and T_∞, C_∞ are the temperature and the concentration of the spices outside the boundary layer respectively, the physical configuration of the problem is shown in **Fig.1**. A uniform magnetic field $\mathbf{B}$ is acting transverse to the plate. Using the relation $\bar{\nabla} \bullet \mathbf{B}$ for the magnetic field, $\mathbf{B} = (B_x, B_y, B_z)$, $B_y = B_0$ has been considered everywhere in the plate (B_0 is a constant). However, for such a fluid, the hall and ion-slip currents will significantly affected the flow in presence of large magnetic fields. The induced magnetic field is neglected since the magnetic Reynolds number of a partially-ionized fluid is very small. If $\mathbf{J} = (J_x, J_y, J_z)$ is the current density, from the relation $\bar{\nabla}.\mathbf{J} = 0$, $J_y =$ constant has been obtained. Since the plate is electrically non-conducting, $J_y = 0$ at the plate and hence zero everywhere. Since the plate is infinite in extent, all physical quantities, except pressure, are functions of y and t only. The equations for the problems are;

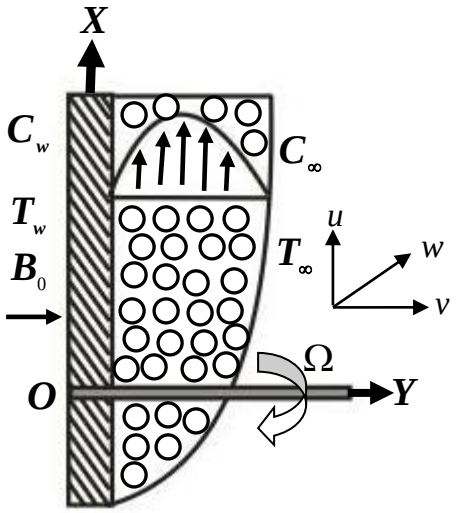

Fig.1 Physical configuration and coordinate system

Continuity equation: $$\frac{\partial v}{\partial y} = 0 \tag{1}$$

Momentum equation:

$$\frac{\partial u}{\partial t} + v\frac{\partial u}{\partial y} = \nu\frac{\partial^2 u}{\partial y^2} + g\beta(T - T_\infty) + g\beta^*(C - C_\infty) + 2\Omega w - \frac{\nu}{k}u - \frac{B_0^2\sigma_e(\alpha_e u + \beta_e w)}{\rho(\alpha_e^2 + \beta_e^2)} \tag{2}$$

$$\frac{\partial w}{\partial t} + v\frac{\partial w}{\partial y} = \nu\frac{\partial^2 w}{\partial y^2} - 2\Omega u - \frac{\nu}{k}w + \frac{B_0^2\sigma_e(\beta_e u - \alpha_e w)}{\rho(\alpha_e^2 + \beta_e^2)} \tag{3}$$

Energy equation: $$\frac{\partial T}{\partial t} + v\frac{\partial T}{\partial y} = \frac{\sigma}{\rho c_p}\frac{\partial^2 T}{\partial y^2} + Q(T_\infty - T) \tag{4}$$

Mass equation: $$\frac{\partial C}{\partial t} + v\frac{\partial C}{\partial y} = D_m\frac{\partial^2 C}{\partial y^2} + \frac{D_m k_T}{T_m}\frac{\partial^2 T}{\partial y^2} \tag{5}$$

The initial and boundary conditions for the model are;

$$u(y,t) = 0, w(y,t) = 0, T(y,t) = T_\infty, C(y,t) = C_\infty \quad \text{for} \quad t \le 0 \tag{6}$$

$$\left.\begin{aligned} u(y,t) = U_0\left[1+\frac{\varepsilon}{2}\left(e^{\text{int}}+e^{-\text{int}}\right)\right], w(y,t)=0, T(y,t)=T_w, C(y,t)=C_w \quad at\ y=0, t>0 \\ u(y,t)=0, w(y,t)=0, T(y,t)=T_\infty, C(y,t)=C_\infty \qquad\qquad at\ y\to\infty, t>0 \end{aligned}\right\} \tag{7}$$

where ε is very small constant quantity and U_0 is uniform velocity, $\alpha_e = 1+\beta_e\beta_i$, β_e is Hall current, β_i is the ion-slip current, y is Cartesian co-ordinate, u and w are the components of flow velocity, g is the local acceleration due to gravity, β is the thermal expansion coefficient, β^* is the concentration expansion coefficient, ν is the kinematic viscosity, k is the magnetic permeability, ρ is the density of the fluid, σ_e is the electrical conductivity, σ is the thermal conductivity, c_p is the specific heat at the constant pressure, D_m is the coefficient of mass diffusivity, Q is the heat absorption quantity, k_T is the thermal diffusion ratio, T_m is the mean fluid temperature and B_0 is the magnetic component in $y-$direction. Now a convenient solution of equation (1) is;

$$v = -v_0 \text{ (constant)} \tag{8}$$

where the constant v_0 represents the normal velocity at the plate which is positive or negative for suction or blowing. Using equation (8), the equations (2)-(5) become;

Momentum equation:

$$\frac{\partial u}{\partial t} - v_0\frac{\partial u}{\partial y} = \nu\frac{\partial^2 u}{\partial y^2} + g\beta(T-T_\infty) + g\beta^*(C-C_\infty) + 2\Omega w - \frac{\nu}{k}u - \frac{B_0^2\sigma_e(\alpha_e u+\beta_e w)}{\rho(\alpha_e^2+\beta_e^2)} \tag{9}$$

$$\frac{\partial w}{\partial t} - v_0\frac{\partial w}{\partial y} = \nu\frac{\partial^2 w}{\partial y^2} - 2\Omega u - \frac{\nu}{k}w + \frac{B_0^2\sigma_e(\beta_e u-\alpha_e w)}{\rho(\alpha_e^2+\beta_e^2)} \tag{10}$$

Energy equation:

$$\frac{\partial T}{\partial t} - v_0\frac{\partial T}{\partial y} = \frac{\sigma}{\rho c_p}\frac{\partial^2 T}{\partial y^2} + Q(T_\infty - T) \tag{11}$$

Mass equation:

$$\frac{\partial C}{\partial t} - v_0\frac{\partial C}{\partial y} = D_m\frac{\partial^2 C}{\partial y^2} + \frac{D_m k_T}{T_m}\frac{\partial^2 T}{\partial y^2} \tag{12}$$

The boundary conditions for the model are;

$$\left.\begin{aligned} u(y,t) = U_0\left[1+\frac{\varepsilon}{2}\left(e^{\text{int}}+e^{-\text{int}}\right)\right], w(y,t)=0, T(y,t)=T_w, C(y,t)=C_w \quad at\ y=0, t>0 \\ u(y,t)=0, w(y,t)=0, T(y,t)=T_\infty, C(y,t)=C_\infty \qquad\qquad at\ y\to\infty, t>0 \end{aligned}\right\} \tag{13}$$

3. Mathematical Formulations

For the purpose of solving the system of equations numerically, the transform of governing equations into non-dimension form are needed, the usual non-dimensional variables are introduced as; $Y = \frac{yU_0}{\nu}$, $U = \frac{u}{U_0}$, $W = \frac{w}{U_0}$, $\tau = \frac{tU_0^2}{\nu}$, $\bar{T} = \frac{T-T_\infty}{T_w-T_\infty}$, $\bar{C} = \frac{C-C_\infty}{C_w-C_\infty}$ (14)

Thus introducing the relation (14) in equation (9)-(12), the following dimensionless differential equations have been obtained as;

$$\frac{\partial U}{\partial \tau}-\lambda\frac{\partial U}{\partial Y}=\frac{\partial^2 U}{\partial Y^2}+G_r\bar{T}+G_m\bar{C}+2RW-\gamma U-\frac{M\left(\alpha_e U+\beta_e W\right)}{\left(\alpha_e^2+\beta_e^2\right)} \tag{15}$$

$$\frac{\partial W}{\partial \tau}-\lambda\frac{\partial W}{\partial Y}=\frac{\partial^2 W}{\partial Y^2}-2RU-\gamma W+\frac{M\left(\beta_e U-\alpha_e W\right)}{\left(\alpha_e^2+\beta_e^2\right)} \tag{16}$$

$$\frac{\partial \bar{T}}{\partial \tau}-\lambda\frac{\partial \bar{T}}{\partial Y}=\frac{\sigma}{\rho c_p \nu}\frac{\partial^2 \bar{T}}{\partial Y^2}-Q\frac{\nu}{U^2}\bar{T},\quad \frac{\partial \bar{T}}{\partial \tau}-\lambda\frac{\partial \bar{T}}{\partial \bar{Y}}=\frac{1}{P_r}\frac{\partial^2 \bar{T}}{\partial Y^2}-\frac{\alpha}{P_r}\bar{T} \tag{17}$$

$$\frac{\partial \bar{C}}{\partial \tau}-\lambda\frac{\partial \bar{C}}{\partial Y}=\frac{1}{S_c}\frac{\partial^2 \bar{C}}{\partial Y^2}+S_0\frac{\partial^2 \bar{T}}{\partial Y^2} \tag{18}$$

where $\lambda=\frac{v_0}{U_0}$ (Suction Parameter), $G_r=\frac{g\beta\left(T_w-T_\infty\right)\nu}{U_0^3}$ (Grashof number), $G_m=\frac{g\beta^*\left(C_w-C_\infty\right)\nu}{U_0^3}$ (modified Grashof number), $M=\frac{\sigma_e B_0^2\nu}{\rho U_0^2}$ (magnetic parameter), $P_r=\frac{\rho c_p \nu}{\sigma}$ (Prandtl number), $S_c=\frac{\nu}{D_m}$ (Schmidt number), $S_0=\frac{D_m k_T\left(T_w-T_\infty\right)}{\nu\left(C_w-C_\infty\right)}$ (Soret number), $R=\frac{\Omega\nu}{U_0^2}$ (rotational parameter), $\alpha=\frac{Q\nu^2\rho c_p}{\sigma U_0^2}$ (Heat source parameter), $\gamma=\frac{\nu^2}{kU_0^2}$ (Permeability of the porous medium)

The corresponding boundary conditions (13) become as;

$$\left.\begin{array}{l}\tau>0\ \ U(Y,\tau)=1+\frac{\varepsilon}{2}\left(e^{i\omega\tau}+e^{-i\omega\tau}\right),\ W(Y,\tau)=0,\ \bar{T}(Y,\tau)=1,\ \bar{C}(Y,\tau)=1\ \ at\ Y=0\\ \qquad U(Y,\tau)=0, W(Y,\tau)=0, \bar{T}(Y,\tau)=0, \bar{C}(Y,\tau)=0 \qquad\qquad at\ Y\to\infty,\end{array}\right\} \tag{19}$$

4. Shear stress, Nusselt and Sherwood number

The Shear stress along x-axis is given by $\tau_x=\mu\left(\frac{\partial u}{\partial y}\right)_{y=0}$ which is proportional to $\left(\frac{\partial U}{\partial Y}\right)_{Y=0}$.

Shear stress along z-axis is given by $\tau_z=\mu\left(\frac{\partial w}{\partial y}\right)_{y=0}$ which is proportional to $\left(\frac{\partial W}{\partial Y}\right)_{Y=0}$.

The Nusselt number N_u which is proportional to $-\left(\frac{\partial \bar{T}}{\partial Y}\right)_{Y=0}$

The Sherwood number, S_h which is proportion to $-\left(\frac{\partial \bar{C}}{\partial Y}\right)_{Y=0}$.

5. Solution Technique

Explicit finite difference method to solve the equations (8)-(11). For these purpose, the region within the boundary layer is divided by some particular lines of Y-axis, where Y-axis is normal to the medium as shown in **Fig.2.** It is assume that the maximum length of the boundary layer is $Y_{\max}(=50)$ as corresponds to $Y \to \infty$ i.e. Y varies from 0 to 50 and the number of grid spacing in Y direction is $m(=400)$, hence the constant mesh size along Y-axis becomes $\Delta Y = 0.13(0 \le Y \le 50)$ with smaller time step, $\Delta t = 0.001$.

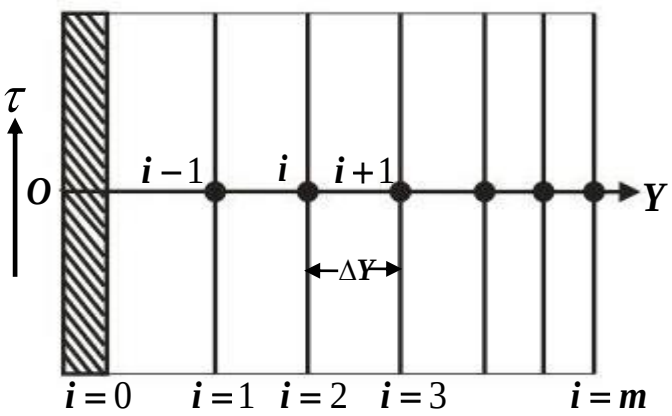

Fig.2 Finite difference grid space

Let $U^{n+1}, W^{n+1}, \bar{T}^{n+1}, \bar{C}^{n+1}$ denoted the values of $U^n, W^n, \bar{T}^n, \bar{C}^n$ at the end of a time-step. Then an appropriate set of finite difference equations corresponding to the equations (15)-(18) are as;

$$\frac{U_i^{n+1}-U_i^n}{\Delta\tau}-\lambda\frac{U_{i+1}^n-U_i^n}{\Delta Y}=G_r\bar{T}_i^n+G_m\bar{C}_i^n+\frac{U_{i+1}^n-2U_i^n+U_{i-1}^n}{(\Delta Y)^2}+2RW_i^n-\gamma U_i^n - \frac{M}{\alpha_e^2+\beta_e^2}\left(\alpha_e U_i^n+\beta_e W_i^n\right) \tag{20}$$

$$\frac{W_i^{n+1}-W_i^n}{\Delta\tau}-\lambda\frac{W_{i+1}^n-W_i^n}{\Delta Y}=\frac{W_{i+1}^n-2W_i^n+W_{i-1}^n}{(\Delta Y)^2}-2RU_i^n-\gamma W_i^n+\frac{M}{\alpha_e^2+\beta_e^2}\left(\beta_e U_i^n-\alpha_e W_i^n\right) \tag{21}$$

$$\frac{\bar{T}_i^{n+1}-\bar{T}_i^n}{\Delta\tau}-\lambda\frac{\bar{T}_{i+1}^n-\bar{T}_i^n}{\Delta Y}=\frac{1}{P_r}\frac{\bar{T}_{i+1}^n-2\bar{T}_i^n+\bar{T}_{i-1}^n}{(\Delta Y)^2}-\frac{\alpha}{P_r}\bar{T}_i^n \tag{22}$$

$$\frac{\bar{C}_i^{n+1}-\bar{C}_i^n}{\Delta\tau}-\lambda\frac{\bar{C}_{i+1}^n-\bar{C}_i^n}{\Delta Y}=\frac{1}{S_c}\frac{\bar{C}_{i+1}^n-2\bar{C}_i^n+\bar{C}_{i-1}^n}{(\Delta Y)^2}+S_0\frac{\bar{T}_{i+1}^n-2\bar{T}_i^n+\bar{T}_{i-1}^n}{(\Delta Y)^2} \tag{23}$$

The boundary conditions are obtained as

$$U_0^n=1,\ W_0^n=0,\ \bar{T}_0^n=1,\ \bar{C}_0^n=1 \tag{24}$$

$U_L^n=0,\ W_L^n=0,\ \bar{T}_L^n=0,\ \bar{C}_L^n=0$ where $L\to\infty$

The numerical values of shear stress, Nusselt number and Sherwood number are evaluated by five-point approximate formula for the derivatives.

The stability conditions of the problem are as follows;

$$\lambda\frac{\Delta\tau}{\Delta Y}+\frac{2}{P_r}\frac{\Delta\tau}{(\Delta Y)^2}+\frac{\alpha\Delta\tau}{2P_r}\le 1,\ \lambda\frac{\Delta\tau}{\Delta Y}+\frac{2}{S_c}\frac{\Delta\tau}{(\Delta Y)^2}\le 1,\lambda\frac{\Delta\tau}{\Delta Y}+\frac{2\Delta\tau}{(\Delta Y)^2}+\frac{\gamma\Delta\tau}{2}\le 1$$

Hence the convergence criteria of the method are $P_r \ge 0.12$ and $S_c \ge 0.12$ (details are not shown for brevity)

6. Results and Discussion

Justification of Grid Space

To verify the effects of grid space for m, the code is true with three different grid space $m = 350, 400, 450$. It is seen that there is a little change between them which are shown in **Fig.3**. According to this situation, the results of velocity, temperature and concentration have been carried out for $m = 400$

Steady state solution

The numerical solutions of the non-linear differential equation (15)-(18) under the boundary conditions (19) have been performed by applying implicit finite difference method. In order to verify the effects of time step size $\Delta\tau$, the programming code is run our model with seven different time step sizes as $\tau = 10, 40, 80, 90, 100, 110, 120$. To get steady–state solutions, the computations have been carried out up to $\tau = 120$. It is observed that, the result of computations for $U, W, \bar{T}$ and $\bar{C}$, however shows little changes after $\tau = 80$. Thus the solutions of all variables for $\tau = 90$ are essentially steady-state. Hence the velocity, temperature and concentration profiles are drawn for
$\tau = 90$ which is shown in **Fig.4.**

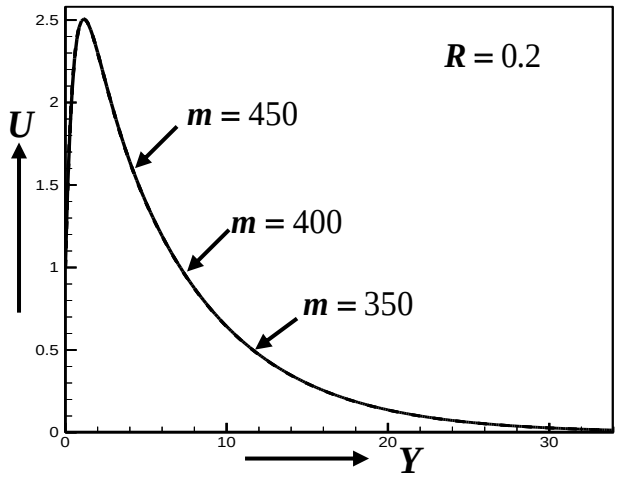

Fig.3 Primary velocity for different grid space of rotational parameter *R*

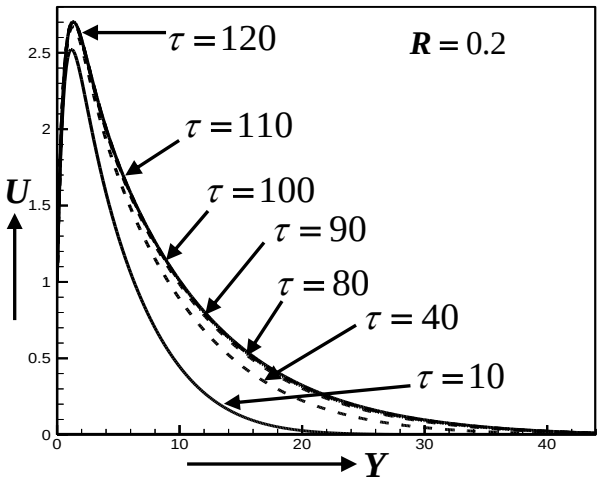

Fig.4 Primary velocity for different time step of rotational parameter *R*

To investigate the physical situation of the problem, the numerical calculation has been carried out for dimensionless primary velocity(U), secondary velocity(W), temperature($\bar{T}$), concentration($\bar{C}$), shear stress in x-direction(τ_x), shear stress in z-direction(τ_z), Nusselt number(N_u) and Sherwood number(S_h) for various values of the parameters such as Hall parameter (β_e), ion-slip parameter(β_i), magnetic parameter(M), rotational parameter (R), Prandtl number(P_r), suction parameter (λ), Schmidt number (S_c), Grashof number(G_r), modified Grashof number(G_m), Soret number(S_0), permeability parameter(γ)and heat source(α). The values for the parameters are chosen arbitrarily in most cases. Some standard values for of the

Prandtl number(P_r) is considered because of the physical importance. These are $P_r = 0.71$ corresponds to air, $P_r = 1.00$ corresponds to electrolyte solution such as salt water and $P_r = 7.00$ corresponds to water at $20^0 C$. For computation $\omega\tau = \frac{\pi}{2}$, $\varepsilon = 0.01$ have been chosen arbitrarily.

Form Fig.5 (a,b) it is seen that primary velocity (U) and shear stress in *x*-direction (τ_x) decrease with increase of heat source parameter α. The effect of increasing the value of α is to decrease the boundary layer which is as expected due to the fact that when heat is absorbed the buoyancy force decreases which retards the flow rate. It is seen that from Fig.6 (a,b) secondary velocity W and shear stress in *z*-direction (τ_z) have opposite behavior with an increase of α. It can be clearly seen that from Fig.7 (a) the temperature profiles decreases with an increase of α. Because when heat is absorbed, the buoyancy force decreases the temperature profiles. Nusselt number $\left[N_u \propto -\left(\frac{\partial \bar{T}}{\partial Y}\right)_{Y=0} \right]$ has reverse effect which is $\propto$ shown in Fig.5(b). The effect of concentration profiles has a negligible increasing effect but Sherwood number $\left[S_h \propto -\left(\frac{\partial \bar{C}}{\partial Y}\right)_{Y=0} \right]$ decreases which is shown in Fig.8(a,b) with an increase of α.

It is observed that in Fig. 9(a,b) and Figs. 11(a,b), primary velocity (U) and shear stress in *x*-direction (τ_x) increase with an increase of Hall parameter β_e and ion-slip parameter β_i. The effective conductivity decrease with increase of β_e and β_i which reduces the magnetic damping force on primary velocity. Similar trend arises in secondary velocity W and shear stress in *z*-direction (τ_z) profiles with increasing β_e which is found form in Fig.10. (a,b). It is found that β_i have decreasing effect on W and τ_z which are shown in Fig.12 (a,b).

From Fig.13 (a,b), it has been seen that the primary velocity U and shear stress in *x*-direction (τ_x) decreases with an increase in magnetic parameter M. This is due to the fact that, the transverse magnetic field normal to the flow direction, has a tendency to create the drag known as the Lorentz force which tends to resist the flow . The secondary velocity W and the shear stress τ_z increase with increase in M which has been illustrated in Fig.14 (a,b). The result indicates that the resulting Lorentzian body force will not act as a drag force as in conventional MHD flows, but as an aiding body force. This will serve to accelerate the secondary fluid velocity.

In Fig.15 (a,b) illustrate that the primary velocity U and shear stress in *x*-direction (τ_x) profiles decrease with the increase of Prandtl number P_r. This is because in the free convection the plate velocity is higher than the adjacent fluid velocity and the momentum boundary layer thickness decreases. Fig.16 (a,b), the secondary velocity W and the shear stress τ_z are increased with the increase of P_r. In Fig.17 (a), the temperature profiles $\bar{T}$ decrease with an increase of P_r. If P_r increases, the thermal diffusivity decreases and these phenomena lead to the decreasing of energy

ability that reduces the thermal boundary layer. The Nusselt number (N_u) does not show approximately any change with an increase of P_r which is shown in Fig.17 (b).

Fig.18 (a,b) are displayed the effect of rotational parameter R on primary velocity U and shear stress in *x*-direction (τ_x) are decreased with increase of R. In fact rotation parameter defines the relative magnitude of the Coriolis force and the viscous force, thus rotation retards primary flow in the boundary layer. Similar behaviors are found on secondary velocity W and shear stress in *z*-direction (τ_z) which are shown in Fig.19 (a,b).

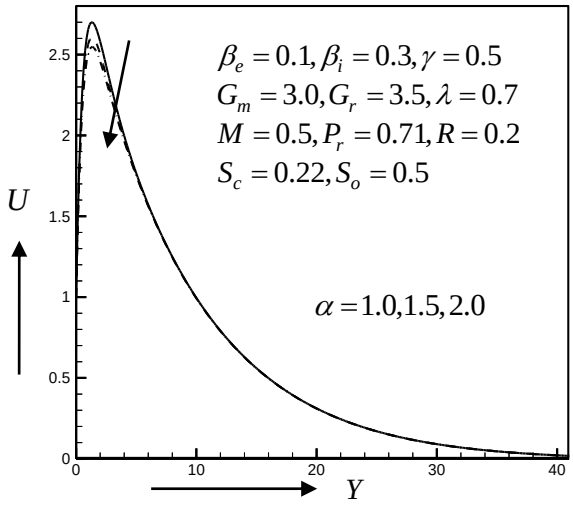

Fig. 5(a) Primary velocity profiles for different values of heat source parameter α

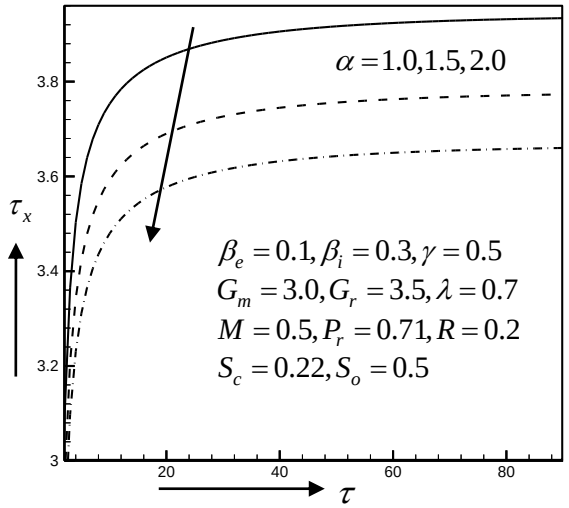

Fig.5(b) Shear stress in *x*-direction for different values of heat source parameter α

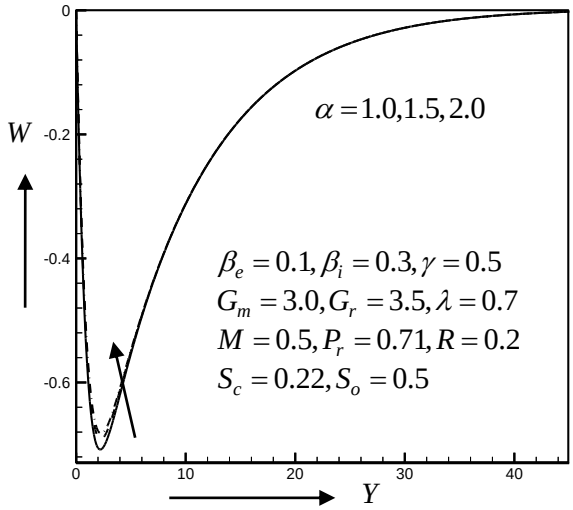

Fig. 6(a) Secondary velocity profiles for different values of heat source parameter α

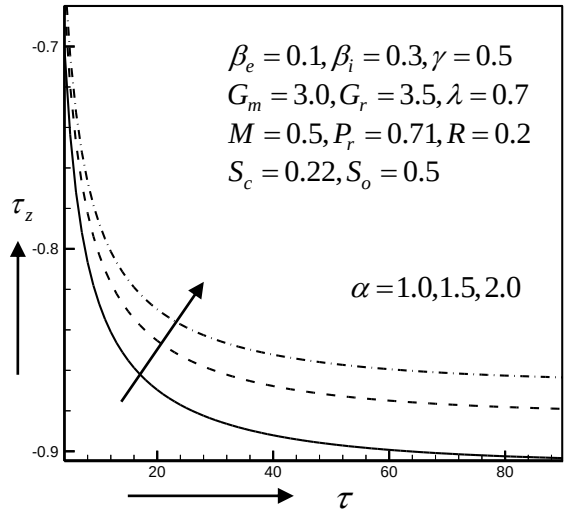

Fig.6(b) Shear stress in *z*-direction for different values of heat source parameter α

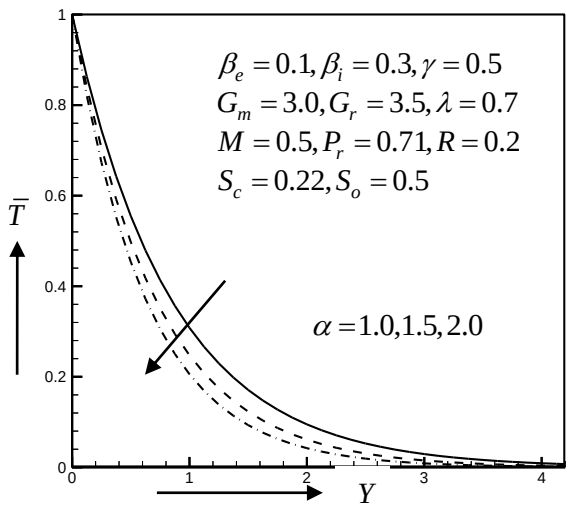

Fig. 7(a) Temperature profiles for different values of heat source parameter α

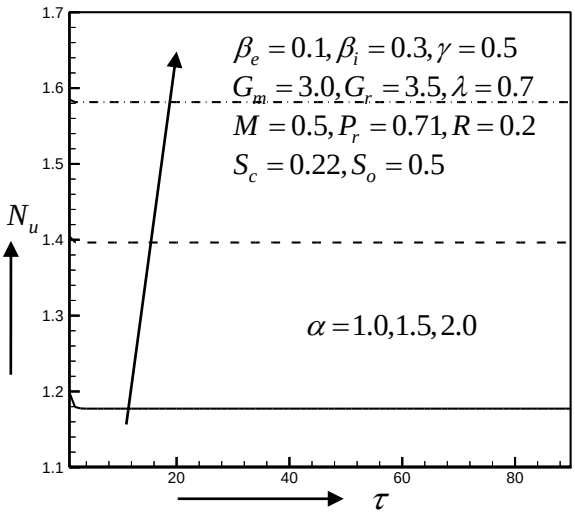

Fig. 7(b) Nusselt number for different values of heat source parameter α

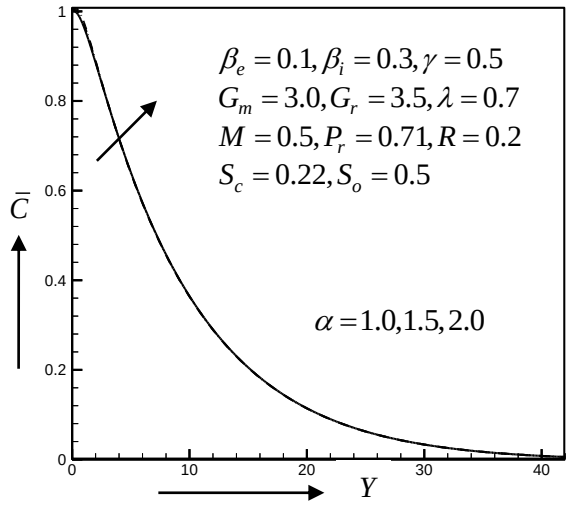

Fig.8(a) Concentration profiles for different values of heat source parameter α

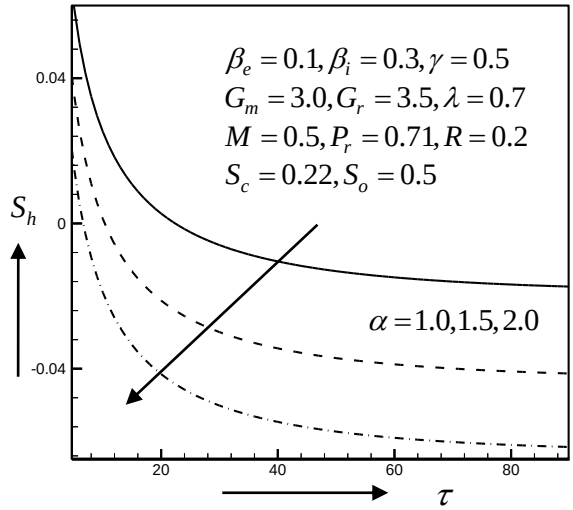

Fig. 8(b) Sherwood number for different values of heat source parameter α

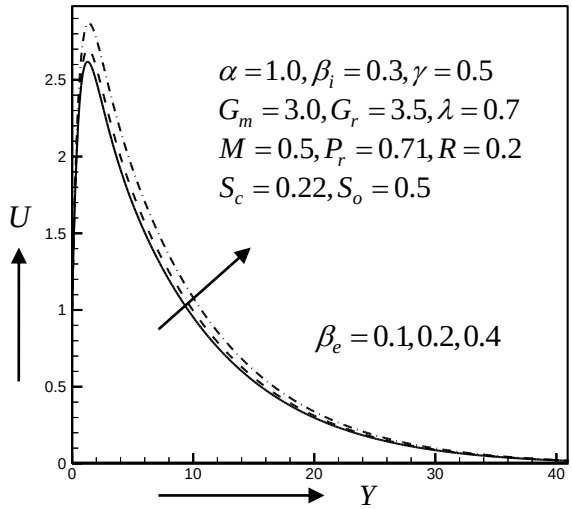

Fig.9(a) Primary velocity profiles for different values of Hall parameter β_e

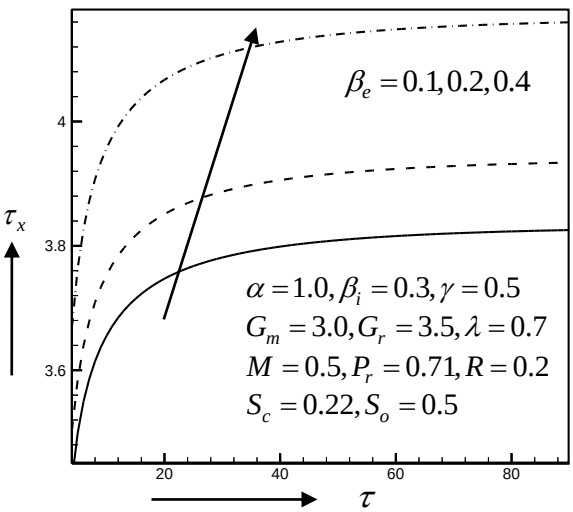

Fig. 9(b) Shear stress in *x*-direction for different values of Hall parameter β_e

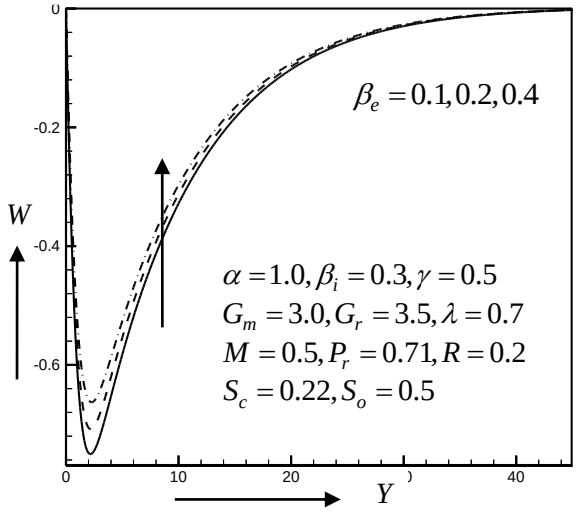

Fig. 10(a) Secondary velocity profiles for different values of Hall parameter β_e

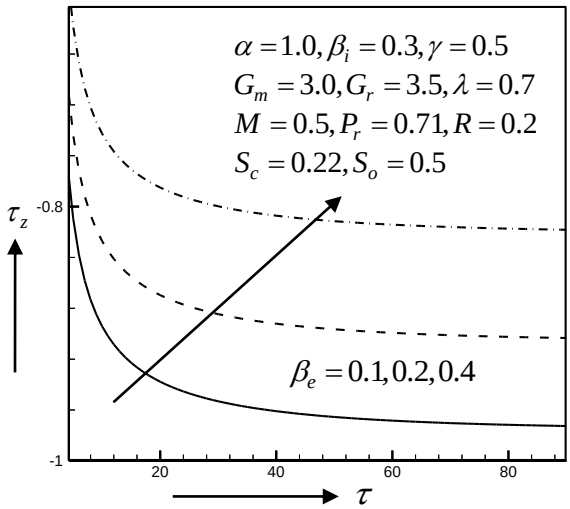

Fig.10(b) Shear stress in *z*-direction for different values of Hall parameter β_e

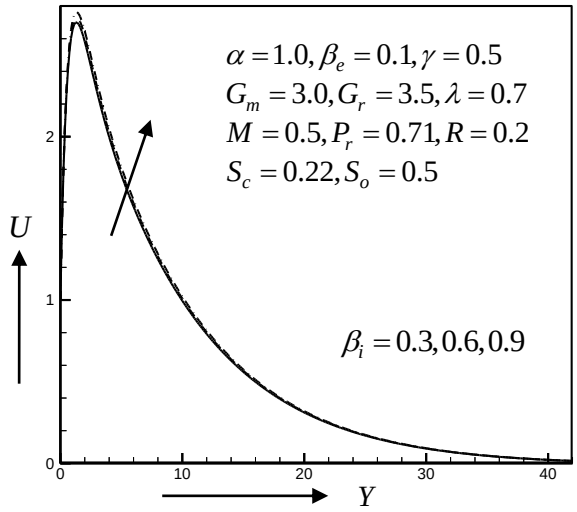

Fig. 11(a) Primary velocity profiles for different values of ion-slip parameter β_i

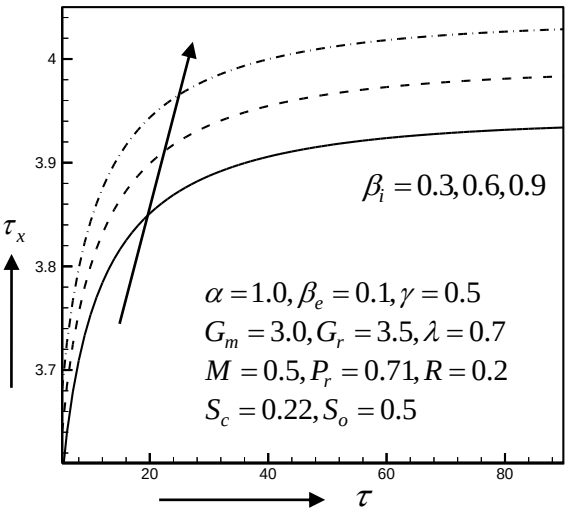

Fig. 11(b) Shear stress in *x*-direction for different values of ion-slip parameter β_i

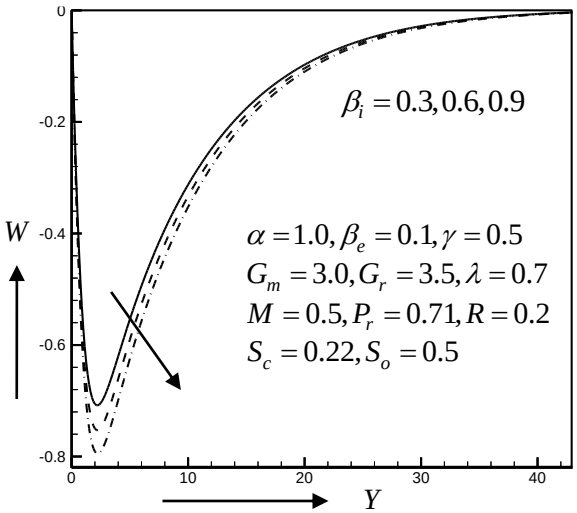

Fig. 12(a)Secondary velocity profiles for different values of ion-slip parameter β_i

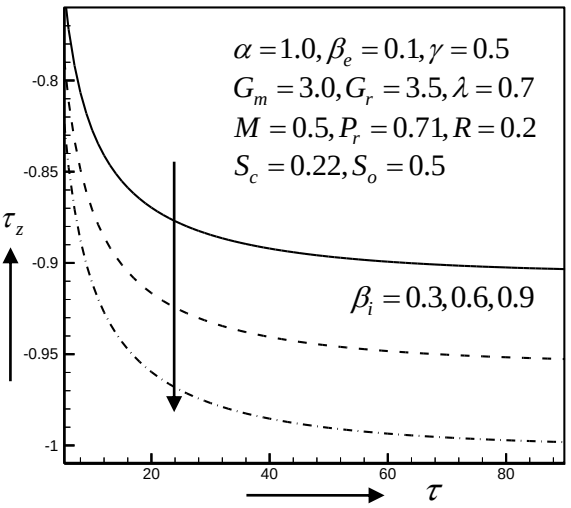

Fig. 12(b) Shear stress in *z*-direction for different values of ion-slip parameter β_i

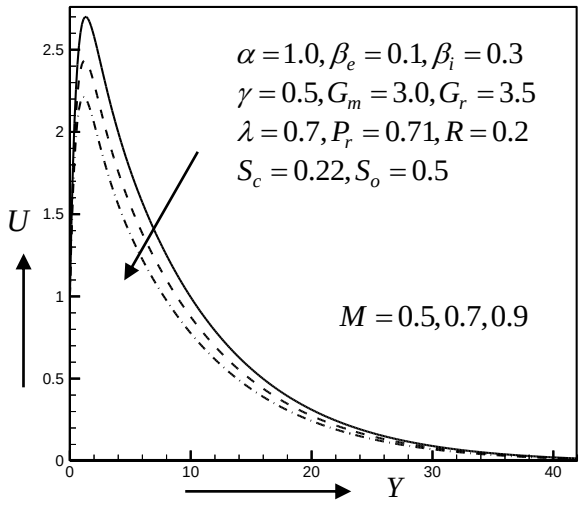

Fig. 13(a) Primary velocity profiles for different values of magnetic parameter M

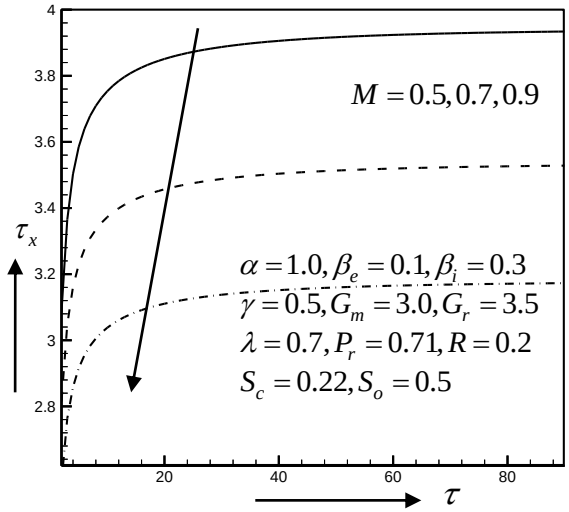

Fig. 13(b) Shear stress in x-direction for different values of magnetic parameter M

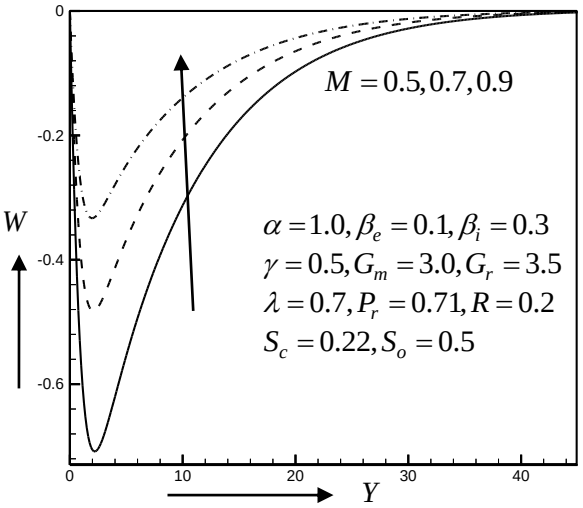

Fig. 14(a) Secondary velocity profiles for different values of magnetic parameter M

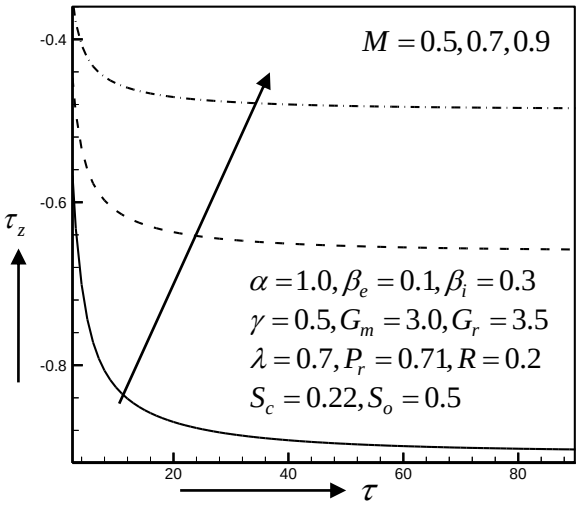

Fig. 14(b) Shear stress in z-direction for different values of magnetic parameter M

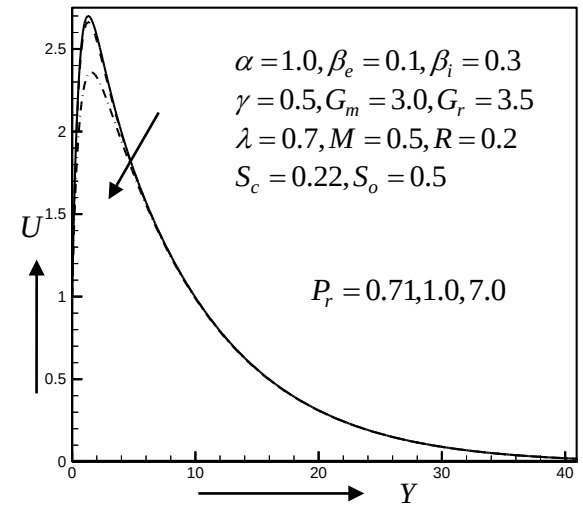

Fig. 15(a) Primary velocity profiles for different values of Prandtl number P_r

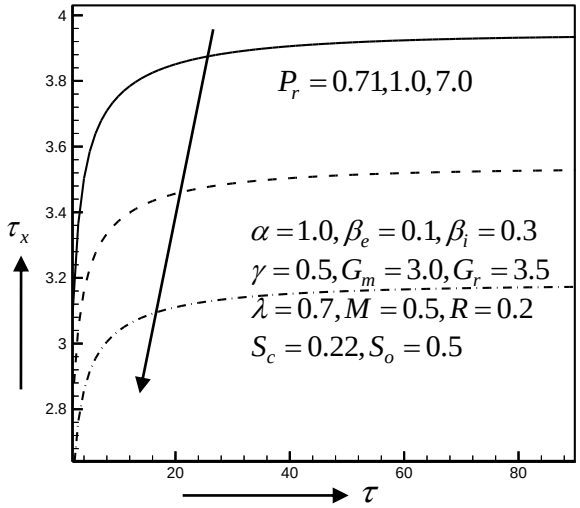

Fig. 15(b) Shear stress in x-direction for different values of Prandtl number P_r

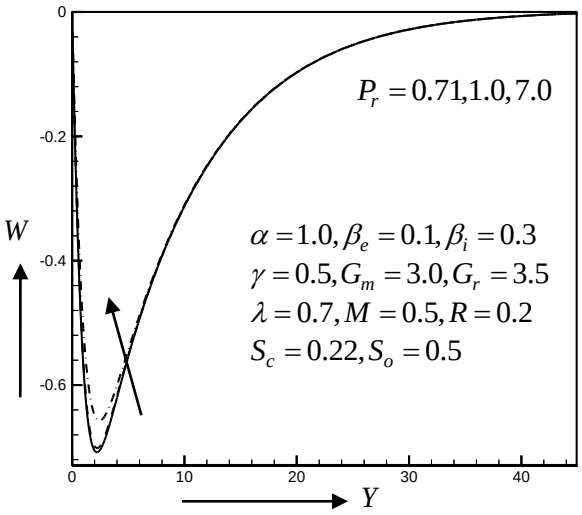

Fig. 16(a) Secondary velocity profiles for different values of Prandtl number P_r

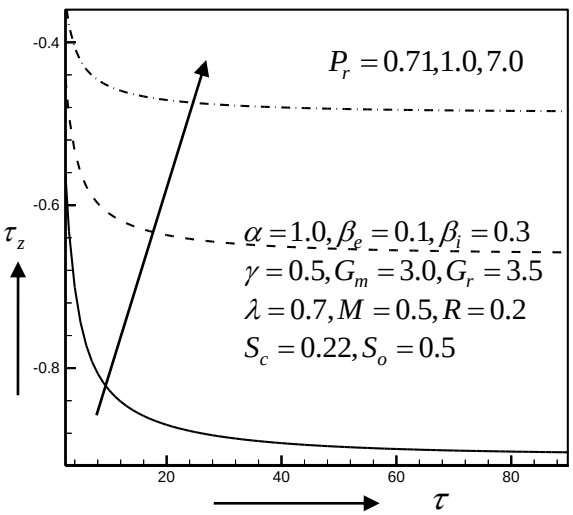

Fig. 16(b) Shear stress in *z*-direction for different values of Prandtl number P_r

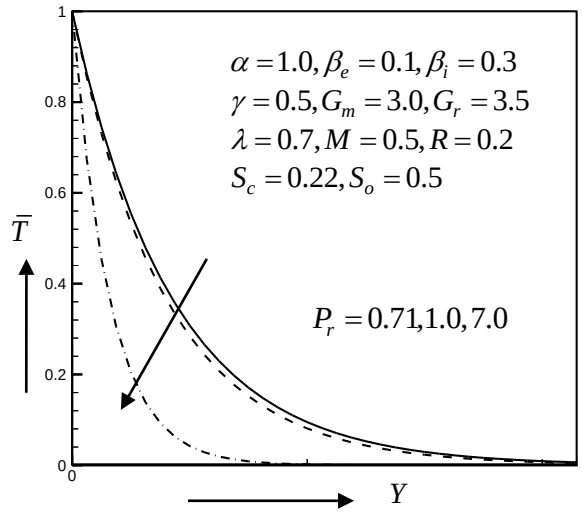

Fig. 17(a) Temperature profiles for different values of Prandtl number P_r

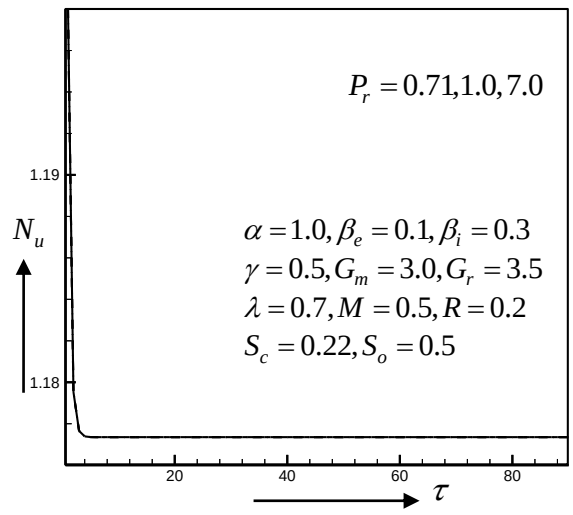

Fig. 17(b) Nusselt number for different values of Prandtl number P_r

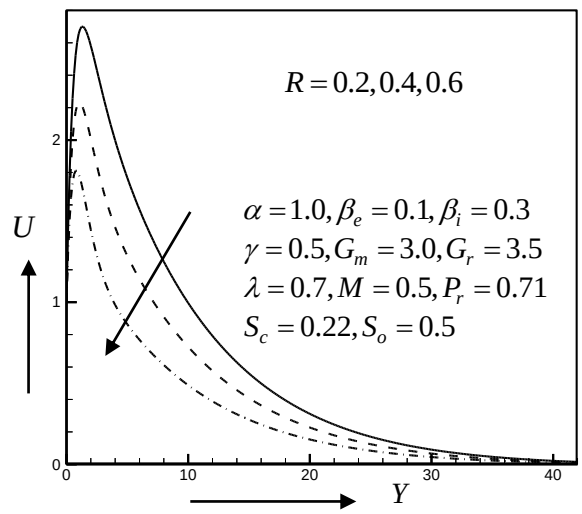

Fig. 18(a) Primary velocity profiles for different values of rotational parameter R

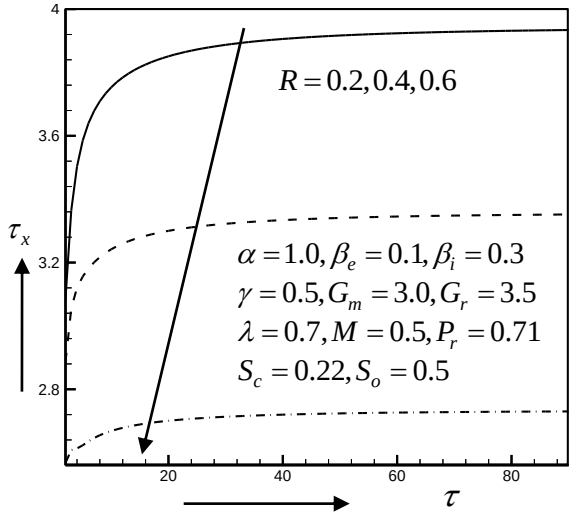

Fig. 18(b) Shear stress in *x*-direction for different values of rotational parameter *R*

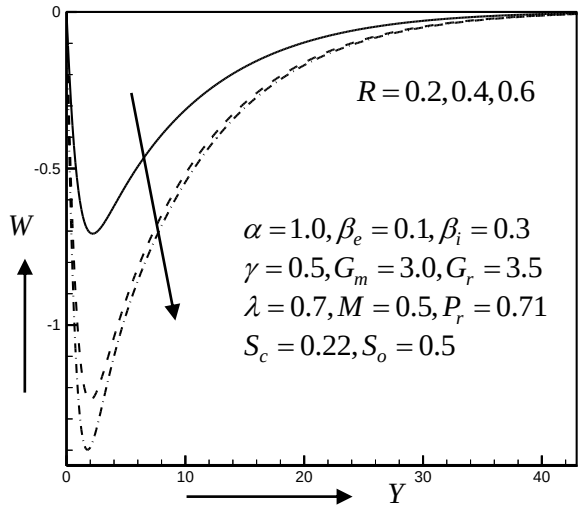

Fig.19(a) Secondary velocity profiles for different values of rotational parameter R

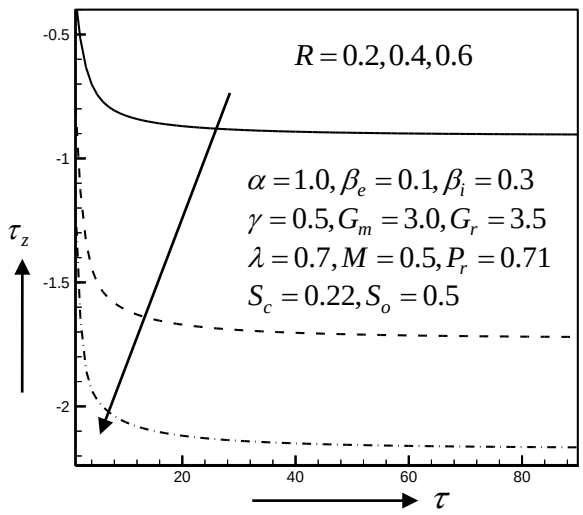

Fig. 19(b) Shear stress in *z*-direction for different values of rotational parameter R

7. Conclusions

In this study, the finite difference solution of unsteady MHD free convection and mass transfer flow through a vertical oscillatory porous plate in a rotating porous medium with hall, ion-slip currents and heat source is investigated. The following conclusions are drawn:

1. Primary velocity, shear stress in *x*-direction are increased for increase β_e, β_i while decrease with the increase of R, P_r, M, α .
2. Secondary velocity, shear stress in *z*-direction are increased for increasing P_r, M, β_e, α while decrease with the increase of β_i, R.
3. Temperature profiles are decreased for increasing P_r, α while Nusselt number increases for α But Prandtl number yields no effect on Nusselt number.
4. Concentration profiles increases for increasing values of α while reverse effect on Sherwood number is observed.

Here magnetic and heat source parameter are used significantly to control the flow and heat transfer characteristics.

References

1. Asghar S., Mohyuddin M.R., and Hayat T., Effects of Hall current and heat transfer on flow due to a pull of eccentric rotating disks, *International Journal of Heat and Mass transfer*. **48**, pp.599-406, 2005.
2. Das, G. C.; Panda J. P; Das, S. S., Finite difference analysis of hydromagnetic flow and heat transfer of an elastico-viscous fluid between two horizontal parallel porous plates, *Modelling, Measurement and Control* B 01; **73**(1):31-44, 2004 .
3. Gupta A.S., Misra J.C., Reza M., Soundalgekar V.M., Flow in the Ekman layer on an oscillating porous plate, *Acta Mechanica*, **165**, pp.1– 16, 2003.

4. Lahurikar R. M., Pohanerkar S. G., Soundalgekar V. M., Birajdar N. S., Mass transfer effects on flow past a vertical oscillating plate with variable temperature, *Heat and Mass Transfer*, **30**(5), pp.309–312, 1995.
5. Ziaul Haque M, Alam M.M, Ferdows M. and Postelnicu A., Micropolar fluid behaviors on steady MHD free convection and mass transfer flow with constant heat and mass fluxes, joule heating and viscous dissipation, *Journal of King Saud University-Engineering Sciences,* **24**, 71-84, 2012.
6. Revankar S. T., Free convection effect on flow past an impulsively started or oscillating infinite vertical plate, *Mechanics Research Comm.*, **27**, 241–246, 2000.
7. Singh, A. K., Hall effects on an oscillatory MHD flow in the Stokes problem past an infinite vertical porous plate. *Astrophysics and Space Science* **93**(1), pp.1–13, 1983.
8. Stokes G. G., On the effect of the internal friction of fluid on the motion of pendulum", *Transactions Cambridge Philosophical Society*, **IX**, 8– 106, 1851.
9. Soundalgekar V.M.,Free convection effects on the flow past a vertical oscillating plate, *Astrophysics and Space Science*, **64**, pp.165– 172, 1979.
10. Soundalgekar V. M., Das U. N., Deka R. K., Free convection effects on MHD flow past an infinite vertical oscillating plate with constant heat flux, *Indian Journal of Mathematics*, **39**(3), pp.195–202, 1997.
11. Turbatu S., Bühler K., Zierep J., New solutions of the II Stokes problem for an oscillating flat plate , *Acta Mechanica*, **129**, pp.25–30, 1998.
12. Vajravelu K. and Hadjinicolaou A., Heat transfer in a viscous fluid over a stretching sheet with viscous dissipation and internal heat generation, *International Communications in Heat and Mass Transfer*, vol. **20**, no. 3, pp. 417–430, 1993.
13. Ziaul Haque and Alam M. M., Micropolar fluid behaviours on unsteady MHD heat and Mass transfer flow with constant heat and mass fluxes, joule heating and viscous dissipation, *AMSE Journal*, Vol. **80**(2), 2011
14. Haque M. and Alam M. M.**,** Transient heat and mass transfer by mixed convection flow from a vertical porous plate with induced magnetic field, constant heat and mass fluxes, *AMSE Journal*, Vol. **78**(4), 2009